Chapter 3
Link, Writhe, and Twist

"In drawing the various closed curves which have a given number of double points, I found it desirable to have some simple mode of ascertaining whether a particular form was a new one, or only a deformation of one of those I had already obtained."
P. G. Tait [337, Page 289].

3.1 Introduction

In many experiments, a pair of coupled rods or strings are subject to various forces and moments. It is natural to ask if any features of the original structure are preserved in the deformed state? The answer is sometimes yes and in this case the preserved feature is often a quantity known as the linking number L_k. While the linking number dates to the early 19th century and finds application in astronomy, electromagnetism, and knot theory, there has been an explosion of interest in L_k starting in the 1950s which can be attributed to two factors. The first factor is Watson and Crick's discovery in the early 1950s of the double helix structure of DNA. The second factor is a series of works [42–44] by Gheorghe Călugăreanu (1902–1976) where he showed that the linking number could be decomposed additively into a twist and a writhe. This result is now known as Călugăreanu's theorem [85, 239] and has enabled deep insights into the differential geometry of pairs of curves which are known as ribbons. This theorem provides a heuristic explanation for coil or loop formation (also known as writhing) of a rod when it is twisted. As a result, it has been applied to experiments on rope, tangled polymers, telephone cords, and DNA in order to gain an understanding of the supercoiling that often accompanies twist (cf. [67–70, 124, 169, 248] and references therein).

Our purpose in this chapter is to give a broad overview on the topics of linking number, twist, writhe, and relative rotations. If we consider the two tangled space curves shown in Figure 3.1, then, by the end of this chapter, the reader should be able to calculate the self-linking of each of the curves and their linking number. Much of

O.M. O'Reilly, *Modeling Nonlinear Problems in the Mechanics of Strings and Rods*,
Interaction of Mechanics and Mathematics, DOI 10.1007/978-3-319-50598-5_3

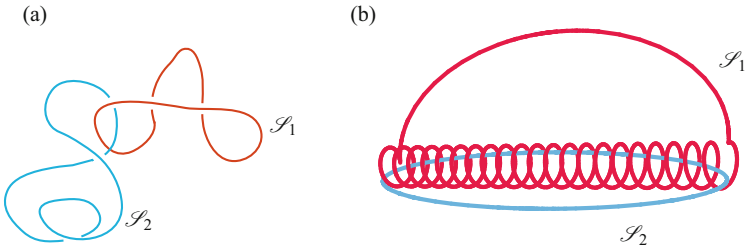

Fig. 3.1 Examples of linked space curves $\mathscr{S}_1$ and $\mathscr{S}_2$. For the curves shown in (a), $L_k(\mathscr{S}_1, \mathscr{S}_2) = \pm 1$ and, for the curves shown in (b), $L_k(\mathscr{S}_1, \mathscr{S}_2) = \pm 21$. These values for the linking numbers were obtained by applying Eqn. (3.34).

what we discuss in this chapter pertains to closed non-self-intersecting space curves. Such curves are also known as knots and there are a wealth of additional analytical tools and perspectives that can be applied to these curves. As we have neither the space nor expertise to cover these topics here, we refer the reader to the accessible text on knot theory by Livingston [210]. In a similar spirit, for further details on the application of the twist, link, and writhe to DNA, we recommend the expository articles by Crick [77] and Pohl [294].

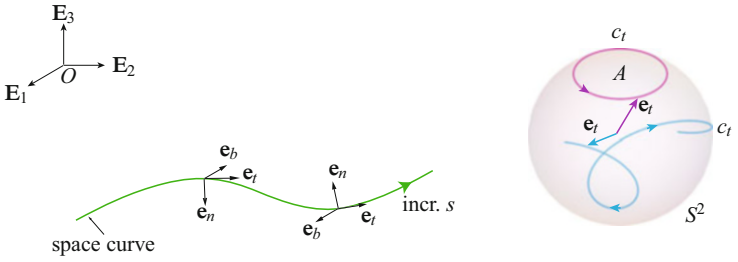

Fig. 3.2 A space curve showing the evolution of the Frenet triad. A pair of representative tantrices or tangent indicatrices c_t on a unit sphere are also shown.

3.2 Space Curves, Ribbons, and Framings

Consider a space curve $\mathscr{S}$ in Euclidean three-dimensional space $\mathbb{E}^3$ (see Figure 3.2). As usual, we define the position vector of a point on the curve:

$$\mathbf{r} = \mathbf{r}(s) = x_1(s)\mathbf{E}_1 + x_2(s)\mathbf{E}_2 + x_3(s)\mathbf{E}_3. \tag{3.1}$$

Recall that the Frenet triad to this curve can be defined by the set of three vectors $\{\mathbf{e}_t, \mathbf{e}_n, \mathbf{e}_b\}$, and that these vectors satisfy the Serret-Frenet relations:

$$\frac{\partial \mathbf{e}_t}{\partial s} = \kappa \mathbf{e}_n, \quad \frac{\partial \mathbf{e}_n}{\partial s} = -\kappa \mathbf{e}_t + \tau \mathbf{e}_b, \quad \frac{\partial \mathbf{e}_b}{\partial s} = -\tau \mathbf{e}_n, \tag{3.2}$$

where τ is the geometric torsion of the space curve and κ is the curvature. You may also recall that the Serret-Frenet relations can be expressed in a compact form by using the Darboux vector $\boldsymbol{\omega}_{\mathrm{SF}} = \tau \mathbf{e}_t + \kappa \mathbf{e}_b$. One undesirable feature of the Frenet frame arises when the curvature vanishes and $\mathbf{e}_n$ is not uniquely defined. As the parameter s passes through such a point, $\mathbf{e}_n$ suffers a discontinuous change.

We can also construct another triad of vectors by defining a unit vector $\mathbf{u}$ which is normal to $\mathbf{e}_t$. The (right-handed orthonormal) triad or frame is completed by defining $\hat{\mathbf{u}} = \mathbf{e}_t \times \mathbf{u}$. If we denote the vector $\boldsymbol{\omega}_{\mathrm{t}}$ as the angular velocity vector associated with this triad, then we have

$$\frac{\partial \mathbf{e}_t}{\partial s} = \omega_3 \mathbf{u} - \omega_2 \hat{\mathbf{u}}, \quad \frac{\partial \mathbf{u}}{\partial s} = -\omega_3 \mathbf{e}_t + \omega_1 \hat{\mathbf{u}}, \quad \frac{\partial \hat{\mathbf{u}}}{\partial s} = \omega_2 \mathbf{e}_t - \omega_1 \mathbf{u}, \tag{3.3}$$

where

$$\boldsymbol{\omega}_{\mathrm{t}} = \omega_1 \mathbf{e}_t + \omega_2 \mathbf{u} + \omega_3 \hat{\mathbf{u}}. \tag{3.4}$$

Examples of the $\{\mathbf{e}_t, \mathbf{u}, \hat{\mathbf{u}}\}$ triad that we shall see later include the triad $\left\{\mathbf{r}', \mathbf{d}_1, \mathbf{d}_2\right\}$ in the theory of the elastica and Kirchhoff's rod theory and the Bishop frame.

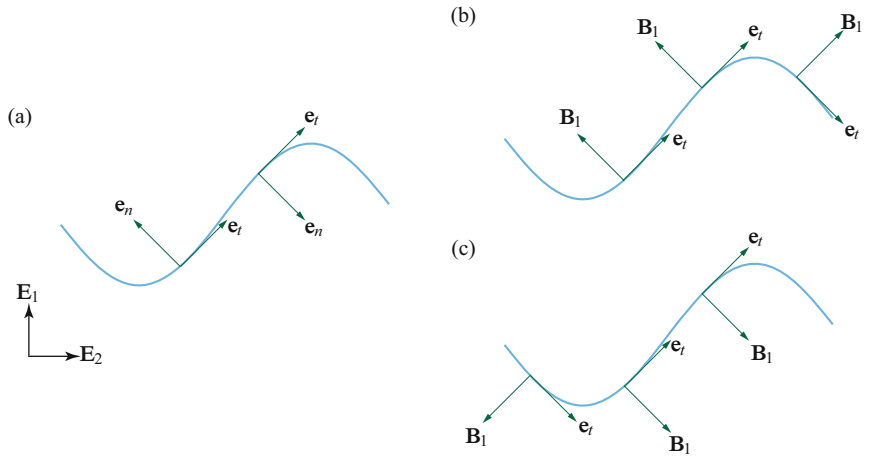

Fig. 3.3 (a) The $\mathbf{e}_t$ and $\mathbf{e}_n$ elements of the Frenet triad for a plane curve with an inflection point. (b) One specification for the element $\mathbf{B}_1$ of the Bishop frame associated with the plane curve. (c) Another specification for the element $\mathbf{B}_1$ of the Bishop frame associated with the plane curve. The binormal vector $\mathbf{e}_b = \mathbf{e}_t \times \mathbf{e}_n$ and the normal vector $\mathbf{B}_2 = \mathbf{e}_t \times \mathbf{B}_1$ are not displayed. Expressions for the unit vectors can be found in Exercise 3.10.

The Bishop frame features the three vectors $\mathbf{e}_t = \mathbf{r}'$, $\mathbf{B}_1$, and $\mathbf{B}_2$ and was introduced in a 1975 paper [28] authored by Bishop. This frame was first used with Kirchhoff's rod theory by Langer and Singer [196] and has since proven to be advantageous particularly in computer graphics (cf. Bergou et al. [22] and Hanson's marvelous book [155, Chapter 20]). Unlike the Frenet frame, Bishop's frame is not unique and is well defined even at points where the curvature of the curve vanishes (see Figure 3.3). To define the Bishop frame, a unit vector $\mathbf{B}_1(s_0)$ lying in the plane normal to $\mathbf{e}_t$ at a chosen location $s = s_0$ on the space curve is chosen. This choice then determines a second unit vector: $\mathbf{B}_2(s_0) = \mathbf{e}_t(s_0) \times \mathbf{B}_1(s_0)$. The vectors $\mathbf{B}_1(s)$ and $\mathbf{B}_2(s)$ are assumed to only change in the direction of $\mathbf{e}_t$. That is, they are said to be relatively parallel to the space curve:

$$\frac{\partial \mathbf{B}_1}{\partial s} = -\kappa_{\mathrm{B}_1}\mathbf{e}_t, \qquad \frac{\partial \mathbf{B}_2}{\partial s} = -\kappa_{\mathrm{B}_2}\mathbf{e}_t. \tag{3.5}$$

Here, the (Bishop) curvatures κ_{B_1} and κ_{B_2} are functions of s and they can have positive and negative values. Because $\mathbf{B}_\alpha$ is normal to $\frac{\partial \mathbf{B}_\alpha}{\partial s}$, the magnitude of the vectors $\mathbf{B}_1$ and $\mathbf{B}_2$ are preserved. For the Frenet triad, we note from Eqn. (3.2) that neither $\mathbf{e}_n$ nor $\mathbf{e}_b$ propagate in a relatively parallel manner along the curve unless the torsion $\tau = 0$. Using the identity $\mathbf{e}_t = \mathbf{B}_1 \times \mathbf{B}_2$, we find that

$$\frac{\partial \mathbf{e}_t}{\partial s} = \kappa_{\mathrm{B}_1}\mathbf{B}_1 + \kappa_{\mathrm{B}_2}\mathbf{B}_2. \tag{3.6}$$

Thus, we can define a vector

$$\boldsymbol{\omega}_{\mathrm{B}} = \kappa_{\mathrm{B}_1}\mathbf{B}_2 - \kappa_{\mathrm{B}_2}\mathbf{B}_1, \tag{3.7}$$

where

$$\frac{\partial \mathbf{e}_t}{\partial s} = \boldsymbol{\omega}_{\mathrm{B}} \times \mathbf{e}_t, \qquad \frac{\partial \mathbf{B}_1}{\partial s} = \boldsymbol{\omega}_{\mathrm{B}} \times \mathbf{B}_1, \qquad \frac{\partial \mathbf{B}_2}{\partial s} = \boldsymbol{\omega}_{\mathrm{B}} \times \mathbf{B}_2. \tag{3.8}$$

As with the Frenet triad, one can define a rotation tensor associated with the vector $\boldsymbol{\omega}_{\mathrm{B}}$, but we do not pause to do so here.

As discussed in [28] and displayed in Figure 3.4, the Bishop frame can be related to the Frenet triad by defining an angle θ_{B}:

$$\begin{aligned} \mathbf{e}_n &= \cos(\theta_{\mathrm{B}})\mathbf{B}_1 + \sin(\theta_{\mathrm{B}})\mathbf{B}_2, \\ \mathbf{e}_b &= -\sin(\theta_{\mathrm{B}})\mathbf{B}_1 + \cos(\theta_{\mathrm{B}})\mathbf{B}_2. \end{aligned} \tag{3.9}$$

With the help of the Serret-Frenet relations (3.2) and assuming that $\kappa \neq 0$, it is straightforward to show how the curvatures κ_{B_1} and κ_{B_2} can be computed from κ and τ:

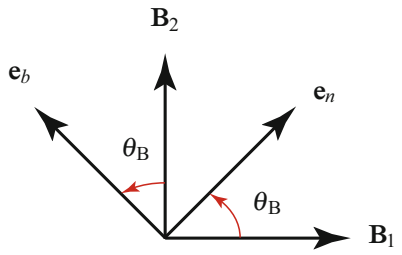

Fig. 3.4 The angle θ_{B} relating the two sets of normal vectors.

$$\kappa_{B_1} = \kappa\cos(\theta_B), \qquad \kappa_{B_2} = \kappa\sin(\theta_B). \tag{3.10}$$

The angle θ_B is found by integrating the relation

$$\tau = \frac{\partial\theta_B}{\partial s}. \tag{3.11}$$

It is interesting to note that θ_B is thereby determined up to an arbitrary constant. Furthermore, the Darboux vector and the vector $\boldsymbol{\omega}_B$ are related as follows:

$$\boldsymbol{\omega}_B = \kappa_{B_1}\mathbf{B}_2 - \kappa_{B_2}\mathbf{B}_1 = \kappa\mathbf{e}_b, \qquad \boldsymbol{\omega}_{SF} = \tau\mathbf{e}_t + \boldsymbol{\omega}_B. \tag{3.12}$$

An example of the computation of the Bishop frame for a plane curve is presented in Exercise 3.10. The results of this exercise are shown graphically in Figure 3.3 and they illustrate our earlier remarks about the nonuniqueness of the Bishop frame.

To illuminate additional features of the Bishop frame, we consider the example of a helical space curve shown in Figure 3.5. As discussed in Section 1.3.4, this curve has a nonvanishing curvature $\kappa = \frac{1}{R(1+\alpha^2)}$ and torsion $\tau = \alpha\kappa$. As a result, we can use an algorithm presented by Guggenheimer [144] to compute the Bishop frame from the Frenet frame[1]:

$$\begin{aligned}
\mathbf{e}_t &= \frac{1}{\sqrt{1+\alpha^2}}(\mathbf{e}_\theta + \alpha\mathbf{E}_3),\\
\mathbf{e}_n &= -\mathbf{e}_r,\\
\mathbf{e}_b &= \frac{1}{\sqrt{1+\alpha^2}}(-\alpha\mathbf{e}_\theta + \mathbf{E}_3).
\end{aligned} \tag{3.13}$$

First, we compute θ_B using the identity $\tau = \frac{\partial\theta_B}{\partial s}$:

$$\begin{aligned}
\theta_B(s) &= \int_{s_0}^{s} \alpha\kappa du + \theta_B(s_0)\\
&= \alpha\kappa(s - s_0) + \theta_B(s_0).
\end{aligned} \tag{3.14}$$

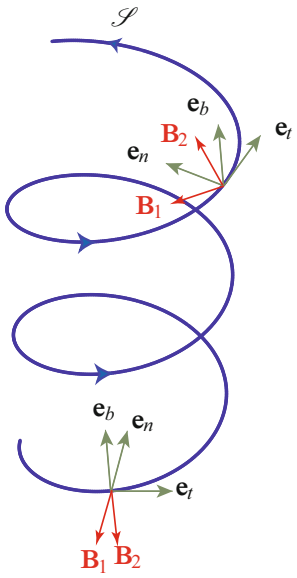

Fig. 3.5 Representative examples of the Frenet and Bishop frames at points on a helical space curve.

Without loss of generality, we choose $s_0 = 0$ and $\theta_B(s_0) = 0$. Inverting the relations (3.9), and using the aforementioned results, we find that

[1] We refer the reader to Bergou et al. [22] and Hanson [155, Chapter 20] for details on the numerical computation of the Bishop frame for space curves.

$$\begin{bmatrix} \mathbf{B}_1 \\ \mathbf{B}_2 \end{bmatrix} = \begin{bmatrix} \cos(\alpha\kappa s) & -\sin(\alpha\kappa s) \\ \sin(\alpha\kappa s) & \cos(\alpha\kappa s) \end{bmatrix} \begin{bmatrix} \mathbf{e}_n \\ \mathbf{e}_b \end{bmatrix}. \tag{3.15}$$

Observe that $\mathbf{B}_1$ and $\mathbf{B}_2$ revolve continuously relative to $\mathbf{e}_n$ and $\mathbf{e}_b$. Furthermore, although κ and τ are constant, the curvatures κ_{B_1} and κ_{B_2} are continuously changing:

$$\kappa_{\mathrm{B}_1} = \kappa\cos(\alpha\kappa s), \qquad \kappa_{\mathrm{B}_2} = \kappa\sin(\alpha\kappa s). \tag{3.16}$$

We leave it as an exercise to show that the Bishop frame obtained by choosing $\theta_B(s_0) \neq 0$ will differ from (3.15) by a rotation through an angle $\theta_B(s_0)$ about $\mathbf{e}_t$ with concomitant changes to the curvatures κ_{B_1} and κ_{B_2}. We close our discussion of the Bishop frame by noting that this frame is also known in the literature as the natural frame, the parallel transport frame, and the relatively parallel adapted frame (cf. [6, 28, 155]).

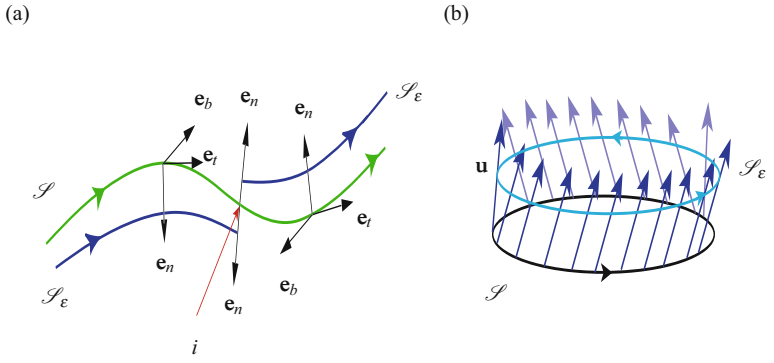

Fig. 3.6 Ribbons constructed from a space curve $\mathscr{S}$. (a) Ribbon constructed using the normal vector $\mathbf{e}_n$ and (b) a ribbon constructed using a vector $\mathbf{u}$. Observe that the ribbon constructed using $\mathbf{e}_n$ is poorly defined at a point of inflection i (where $\frac{\partial^2 \mathbf{r}}{\partial s^2} = \mathbf{0}$ or, equivalently, $\kappa = 0$). This well-known issue [42, 239] arises because $\mathbf{e}_n$ suffers a discontinuity at i: $[\![\mathbf{e}_n]\!] \neq \mathbf{0}$.

3.2.1 Ribbons

The vector $\mathbf{u}$ featuring in Eqn. (3.3) can be used to define another curve:

$$\mathscr{S}_\varepsilon : \mathbf{r}_\varepsilon = \mathbf{r}(s) + \varepsilon\mathbf{u}(s). \tag{3.17}$$

If we consider the union of the points on $\mathscr{S}$, $\mathscr{S}_\varepsilon$, and the points along $\varepsilon\mathbf{u}$ connecting them, then we will have defined a ruled surface (cf. Figure 3.6). In differential geometry, this surface is known as a ribbon and we shall assume in the sequel that ε is sufficiently small so that the two curves $\mathscr{S}$ and $\mathscr{S}_\varepsilon$ do not intersect. We also

note that if $\mathscr{S}$ is closed and does not intersect itself, then we assume that $\mathscr{S}_\varepsilon$ is constructed to have these properties too. In many applications of the ideas presented in this chapter the pair of curves $\mathscr{S}$ and $\mathscr{S}_\varepsilon$ model the sugar-phosphate backbone curves of DNA.

3.2.2 Gauss-Bonnet Theorem

It is often surprisingly useful to map the tangent vector to the space curve so that its tip describes a curve on a unit sphere S^2. The associated curve is known as the tangent indicatrix or tantrix c_t and representative examples are shown in Figures 3.2 and 3.7. When c_t forms a closed curve on the sphere, then it also encloses a solid angle A.[2] The celebrated Gauss-Bonnet theorem, named after Carl F. Gauss (1777–1855) and Pierre O. Bonnet (1819–1892), we shall present relates this solid angle to properties of the tantrix. Dating to Kelvin and Tait [341, Section 123] in 1867, this theorem has also been used as a novel method to determine relative rotations of the cross sections of rods.

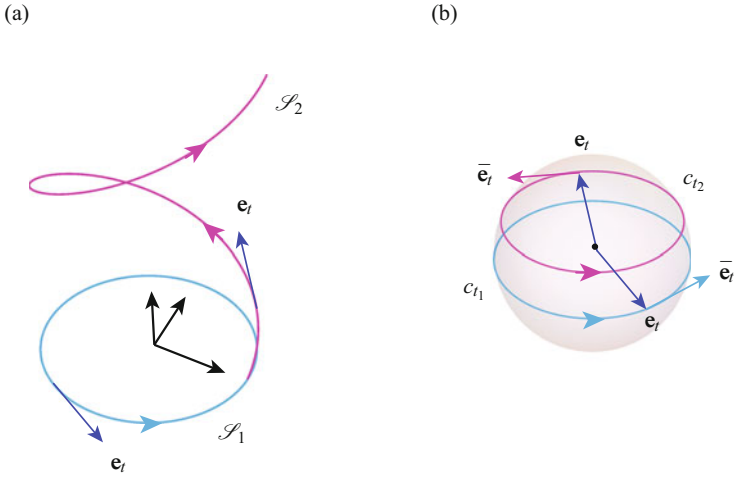

Fig. 3.7 A pair of space curves and their associated tangent indicatrices. In (a) the curves $\mathscr{S}_1$ is a circle and $\mathscr{S}_2$ is a helix. The respective tangent indicatrices c_{t_1} and c_{t_2} are shown in (b).

Consider the case where c_t forms a closed curve on S^2 and let us embed this sphere in $\mathbb{E}^3$ with $\mathbf{E}_3$ passing along the polar axis. We put coordinates on the sphere using a set of spherical polar coordinates $\{\phi_1 \in [0, 2\pi], \phi_2 \in [0, \pi]\}$ where $\phi_2 = 0$

[2] The total surface area of a unit sphere is 4π. In topology, the area A in Figure 3.2 is known as a solid angle.

and π at the north and south poles of the sphere, respectively. With this coordinate system in place, the tangent space at a point (ϕ_1, ϕ_2) on the sphere is spanned by the vectors $\mathbf{e}_{\phi_1}$ and $\mathbf{e}_{\phi_2}$:

$$\begin{aligned} \mathbf{e}_{\phi_1} &= -\sin(\phi_1)\mathbf{E}_1 + \cos(\phi_1)\mathbf{E}_2, \\ \mathbf{e}_{\phi_2} &= \cos(\phi_2)\cos(\phi_1)\mathbf{E}_1 + \cos(\phi_2)\sin(\phi_1)\mathbf{E}_2 - \sin(\phi_2)\mathbf{E}_3, \end{aligned} \tag{3.18}$$

where

$$\mathbf{e}_t = \sin(\phi_2)\cos(\phi_1)\mathbf{E}_1 + \sin(\phi_2)\sin(\phi_1)\mathbf{E}_2 + \cos(\phi_2)\mathbf{E}_3. \tag{3.19}$$

Examining the rate of change of $\mathbf{e}_t$, we find that

$$\begin{aligned} \frac{\partial \mathbf{e}_t}{\partial s} &= \frac{\partial \phi_1}{\partial s}\sin(\phi_2)\mathbf{e}_{\phi_1} + \frac{\partial \phi_2}{\partial s}\mathbf{e}_{\phi_2}, \\ \kappa^2 &= \left(\frac{\partial \phi_2}{\partial s}\right)^2 + \left(\frac{\partial \phi_1}{\partial s}\right)^2 \sin^2(\phi_2). \end{aligned} \tag{3.20}$$

Thus, an expression for the unit tangent vector $\bar{\mathbf{e}}_t$ to c_t and the relation between the arc-length parameter s of $\mathscr{S}$ and the arc-length parameter $\bar{s}$ of c_t can be established:

$$\bar{\mathbf{e}}_t = \frac{1}{\kappa}\frac{\partial \mathbf{e}_t}{\partial s}, \qquad \frac{ds}{d\bar{s}} = \frac{1}{\kappa}. \tag{3.21}$$

An expression for the curvature vector $\boldsymbol{\kappa} = \frac{\partial \bar{\mathbf{e}}_t}{\partial \bar{s}}$ can also be computed. The geodesic curvature κ_g of c_t on S^2 is defined as the rate of change of $\bar{\mathbf{e}}_t$ in the tangent plane spanned by $\mathbf{e}_{\phi_1}$ and $\mathbf{e}_{\phi_2}$. Using the properties of the scalar triple product and the definition (1.9) of the geometric torsion, we perform the following set of manipulations:

$$\begin{aligned} \kappa_g &= \left[\mathbf{e}_t, \bar{\mathbf{e}}_t, \frac{\partial \bar{\mathbf{e}}_t}{\partial \bar{s}}\right] \\ &= \left[\mathbf{e}_t, \frac{1}{\kappa}\frac{\partial \mathbf{e}_t}{\partial s}, \frac{1}{\kappa^2}\frac{\partial^2 \mathbf{e}_t}{\partial s^2}\right], \end{aligned} \tag{3.22}$$

and arrive at the conclusions that

$$\kappa_g = \frac{\tau}{\kappa}, \qquad \kappa_g d\bar{s} = \tau ds. \tag{3.23}$$

In the event that the tangent indicatrix describes a great circle (which is the case if $\mathscr{S}$ is a circle), then $\tau = 0$ and consequently $\kappa_g = 0$. This case illustrates the result that $\kappa_g = 0$ when c_t is a geodesic on S^2.

Suppose that c_t is closed, then the Gauss-Bonnet theorem for this case states that the solid angle A enclosed by this curve satisfies the identity

$$\oint_{c_t} \kappa_g d\bar{s} + A = 2\pi \qquad \text{modulo } 4\pi. \tag{3.24}$$

In the event that c_t has corners with exterior angles $\alpha_k\,(k=1,\ldots,n)$, then a term $\sum_{k=1}^{n}\alpha_k$ is added to the left-hand side of Eqn. (3.24) (cf., e.g., [234, Page 192, Exercise 15]). Although our interest in applications of the Gauss-Bonnet theorem is restricted to curves on the sphere S^2, the theorem has a far broader range of application. We refer the reader to texts on differential geometry such as [188, 257] for details on more general forms of this classical theorem.

Let us now apply Eqn. (3.24) to the helix discussed earlier in Section 1.3.4. We recall that the curvature κ and torsion τ of the helix are

$$\kappa=\frac{1}{R\left(1+\alpha^2\right)}=\frac{1}{R}\cos^2(\varsigma),\qquad \tau=\frac{\alpha}{R\left(1+\alpha^2\right)}=\frac{1}{R}\cos(\varsigma)\sin(\varsigma), \tag{3.25}$$

where $\varsigma=\arctan(\alpha)$ is the pitch angle of the helix. Thus, using the identity $\kappa_g=\tau/\kappa$, the geodesic curvature of the tangent indicatrix is

$$\kappa_g=\alpha. \tag{3.26}$$

If we examine the solid angle enclosed by the tantrix then it is easy to verify that Eqn. (3.24) holds. For the circle shown in Figure 3.7(a), c_{t_1} is a great circle with $\bar{s}\in[0,2\pi]$ and so $\kappa_g=0$. By inspection, the solid angle is 2π in agreement with Eqn. (3.24). On the other hand for the helix shown in Figure 3.7(a), $\kappa_g=\alpha$, $\bar{s}\in\left[0,2\pi/\sqrt{1+\alpha^2}\right]$, and the solid angle A enclosed by c_{t_2} as given by Eqn. (3.24) and those obtained by directly computing the area of the spherical cap above c_{t_2} are in agreement: $A=2\pi\left(1-\alpha/\sqrt{1+\alpha^2}\right)$.

3.3 Gauss' Linking Number of Two Space Curves

The earliest measure of how much two curves wind around each other was developed in the early 19th century by Gauss. Although he first described this measure in his notebook in 1833, it was published posthumously in 1867. The derivation for Gauss' measure, which is known as the linking number, is not discussed in his notebook and the first derivation, motivated by his studies on electromagnetic induction, was supplied by James C. Maxwell (1831–1879) in 1867.[3]

Gauss' linking number pertains to two closed nonintersecting space curves $\mathscr{S}_1$ and $\mathscr{S}_2$ such as the pairs shown in Figures 3.1 and 3.8. If the curves are respectively parameterized by $s_1\in[0,2\pi]$ and $s_2\in[0,2\pi]$, then we can define the following unit vector $\mathbf{e}$ which points from a point with position vector $\mathbf{r}_2(s_2)$ on $\mathscr{S}_2$ to a point on $\mathscr{S}_1$ with position vector $\mathbf{r}_1(s_1)$:

[3] Our historical comments in this section are based entirely on the (recent) insightful papers by Epple [95, 96] and Ricca and Nipoti [301]. The latter paper contains a translation of the page in Gauss' notebook where Eqn. (3.28) is presented as well as copies of letters from Maxwell to Tait discussing the linking number.

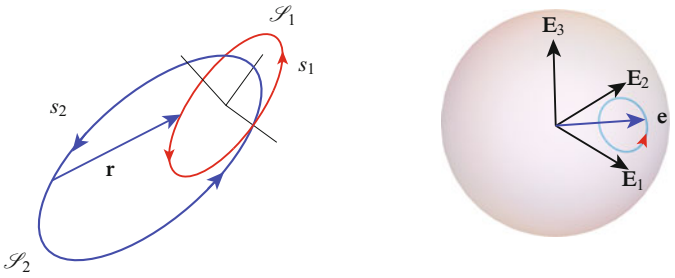

Fig. 3.8 An example of a pair of space curves $\mathscr{S}_1$ and $\mathscr{S}_2$ illustrating the vector $\mathbf{r} = \mathbf{r}_1(s_1) - \mathbf{r}_2(s_2)$ and the associated normalized unit vector $\mathbf{e} = \frac{\mathbf{r}}{\|\mathbf{r}\|}$. For the example shown in this figure, the space curves are defined by Eqn. (3.31) with $c = -1.5$. For the example of the Gauss map that is displayed, $s_2 = \frac{3\pi}{4}$ and s_1 varies from 0 to 2π.

$$\mathbf{e}(s_1, s_2) = \frac{\mathbf{r}_1(s_1) - \mathbf{r}_2(s_2)}{\|\mathbf{r}_1(s_1) - \mathbf{r}_2(s_2)\|}. \tag{3.27}$$

The linking number $L_k(\mathscr{S}_1, \mathscr{S}_2)$ between the two curves, which measures how much $\mathscr{S}_1$ winds around $\mathscr{S}_2$, is then defined by the integral[4]

$$L_k(\mathscr{S}_1, \mathscr{S}_2) = \frac{1}{4\pi} \oint_{\mathscr{S}_1} \oint_{\mathscr{S}_2} f(s_1, s_2)\, ds_1 ds_2, \tag{3.28}$$

where

$$f(s_1, s_2) = \frac{(\mathbf{e}_{t_1}(s_1) \times \mathbf{e}_{t_2}(s_2)) \cdot \mathbf{e}(s_1, s_2)}{\|\mathbf{r}_1(s_1) - \mathbf{r}_2(s_2)\|^2}. \tag{3.29}$$

Here, $\mathbf{e}_{t_1}$ is the unit tangent vector to $\mathscr{S}_1$ and $\mathbf{e}_{t_2}$ is the unit tangent vector to $\mathscr{S}_2$. As Gauss noted, and which we can also readily observe from the definition,

$$L_k(\mathscr{S}_1, \mathscr{S}_2) = L_k(\mathscr{S}_2, \mathscr{S}_1). \tag{3.30}$$

Gauss also noted (a remarkable result which is far from apparent) that $L_k(\mathscr{S}_1, \mathscr{S}_2)$ is integer-valued. The function $\mathbf{e}$ is known as the Gauss map. As illustrated in Figure 3.8, its value can be visualized by plotting the locus of $\mathbf{e}(s_1, s_2)$ on the unit sphere.

To illuminate the linking number defined by Eqn. (3.28) let us consider the pair of ellipses shown in Figure 3.9:

$$\begin{aligned} \mathbf{r}_1(s_1) &= \cos(s_1)\mathbf{E}_1 + 2\sin(s_1)\mathbf{E}_2, \\ \mathbf{r}_2(s_1) &= (3\cos(s_1) + c)\mathbf{E}_2 + 2\sin(s_1)\mathbf{E}_3, \end{aligned} \tag{3.31}$$

[4] Our convention for writing $L_k(\mathscr{S}_1, \mathscr{S}_2)$ is taken from Spivak [329, Problem 8.28, Page 402] and differs from Gauss' original prescription by a minus sign. As a result, our computations using Eqn. (3.28), such as the results shown in Figure 3.9, agree with those found by counting the signed crossings using Eqn. (3.34).

where c is a constant. We consider three cases: $c = -1.5$, $c = 0$, and $c = 1.5$. For the first and third of these cases, $\mathscr{S}_2$ can be considered to wind once around $\mathscr{S}_1$ while in the second case, the space curves do not cross. Numerically evaluating the double integral in Eqn. (3.28), we find the values of $L_k(\mathscr{S}_1, \mathscr{S}_2)$ predicted for the respective cases are 1, 0, and -1.

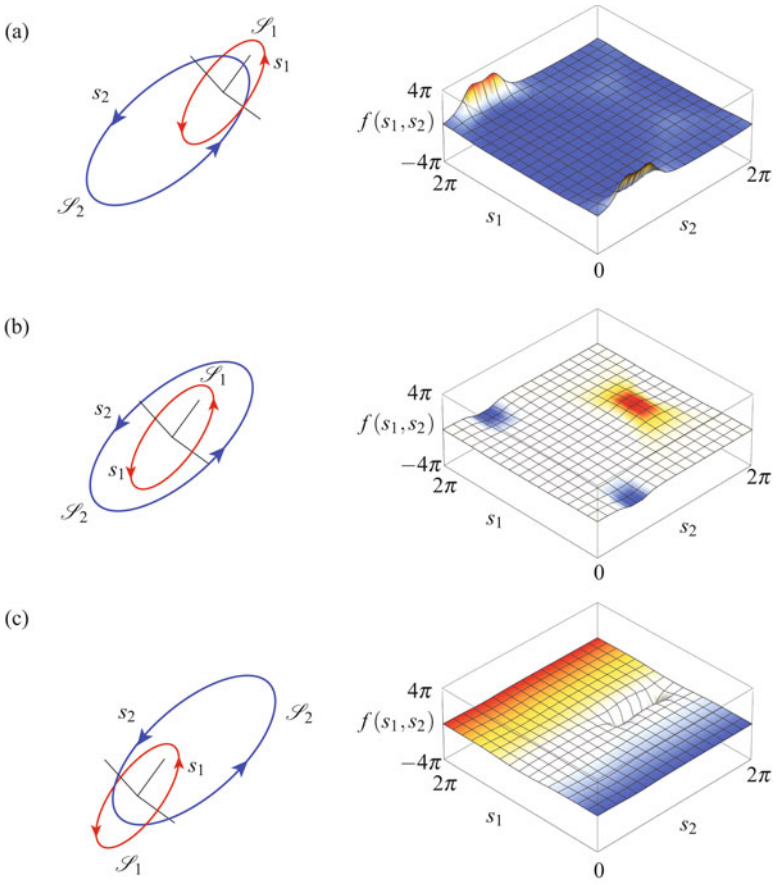

Fig. 3.9 Three examples of a pair of space curves $\mathscr{S}_1$ and $\mathscr{S}_2$ showing the behavior of the associated linking function $f(s_1,s_2)$ (cf. Eqn. (3.29)). For (a), $c = -1.5$ and $L_k(\mathscr{S}_1,\mathscr{S}_2) = 1$; for (b), $c = 0.0$ and $L_k(\mathscr{S}_1,\mathscr{S}_2) = 0$; and for (c), $c = 1.5$ and $L_k(\mathscr{S}_1,\mathscr{S}_2) = -1$. The linking number $L_k(\mathscr{S}_1,\mathscr{S}_2)$ is defined by Eqn. (3.28) and the constant c is used to specify the curve $\mathscr{S}_2$ (cf. Eqn. (3.31)).

While Gauss did not provide a derivation for L_k, Maxwell [233, Sections 417–422], who was working on establishing an expression for the work done by a magnetic pole while moving in a closed curve around a closed electric circuit, made several interesting observations. Among others, he noted that the integrand can be

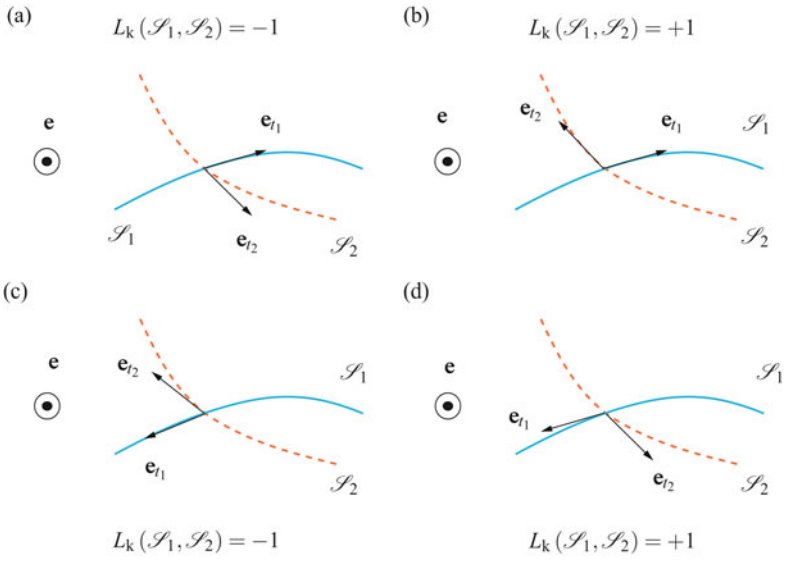

Fig. 3.10 The two distinct values of a signed crossing at a point of transversal crossing of two space curves and the pair of situations associated with each value. For (a) and (c), $L_k(\mathscr{S}_1,\mathscr{S}_2) = -1$ and $L_k(\mathscr{S}_1,\mathscr{S}_2) = +1$ for (b) and (d). In this figure, the dotted curve $\mathscr{S}_2$ is assumed to pass underneath the solid curve $\mathscr{S}_1$ at the crossing point, and, as a result, the vector $\mathbf{e}$ (cf. Eqn. (3.27)) points out of the page. If the solid curve passes underneath the dashed curve, then the linking numbers shown in this figure would change sign.

viewed as the volume formed in part by the solid angle spanned by the partial derivatives of $\mathbf{e}(s_1,s_2)$:

$$-\mathbf{e}\cdot\left(\frac{\partial \mathbf{e}}{\partial s_1}\times\frac{\partial \mathbf{e}}{\partial s_2}\right)ds_1ds_2 = \frac{(\mathbf{e}_{t_1}(s_1)\times\mathbf{e}_{t_2}(s_2))\cdot\mathbf{e}(s_1,s_2)}{\|\mathbf{r}_1(s_1)-\mathbf{r}_2(s_2)\|^2}ds_1ds_2. \tag{3.32}$$

As a result, the linking number (3.28) appears in studies on electromagnetism. Maxwell also noted a geometric method which can be used to evaluate the integrals in Eqn. (3.28). Before we discuss this method, we note that there are six other equivalent methods (up to a sign) of calculating $L_k(\mathscr{S}_1,\mathscr{S}_2)$.[5]

A geometric method for computing the linking number L_k uses signed crossings. Following [257, 294], suppose that the plane projection of the two curves $\mathscr{S}_1$ and $\mathscr{S}_2$ results in a point of crossing $\mathscr{P}$. This crossing corresponds to $\mathbf{r}_1(s_1)$ on $\mathscr{S}_1$ and $\mathbf{r}_2(s_2)$ on $\mathscr{S}_2$. Suppose that $\mathscr{S}_1$ is above $\mathscr{S}_2$ at this crossing point (see Figure 3.10). We use the unit vector $\mathbf{e}$ which points from $\mathscr{S}_2$ to $\mathscr{S}_1$: Then, the index $J(\mathscr{P})$ at the crossing point $\mathscr{P}$ is defined as

[5] These methods are discussed in several places in the literature and summarized in Rolfsen's text [303, Chapter 5, Section D].

$$J(\mathscr{P}) = 1 \text{ if } [\mathbf{e}_{t_1}(s_1), \mathbf{e}_{t_2}(s_2), \mathbf{e}] > 0,$$
$$J(\mathscr{P}) = -1 \text{ if } [\mathbf{e}_{t_1}(s_1), \mathbf{e}_{t_2}(s_2), \mathbf{e}] < 0. \tag{3.33}$$

The linking number of the curves is then defined as half the sum of the indices over all crossing points:

$$L_{\mathrm{k}}(\mathscr{S}_1, \mathscr{S}_2) = \frac{1}{2} \sum_{\mathscr{P}} J(\mathscr{P}). \tag{3.34}$$

Notice that the linking number depends on the handedness of the triad $\{\mathbf{e}_{t_1}, \mathbf{e}_{t_2}, \mathbf{e}\}$. We leave it as an exercise to verify that Eqn. (3.34) agrees with the results found for the curves in Figure 3.9. The latter results were obtained by numerically integrating Eqn. (3.28).

The linking number of two closed curves which have no points of intersection has several properties which we now summarize:

(i) The linking number is an integer $(\ldots, -2, -1, 0, 1, 2, \ldots)$.
(ii) $L_{\mathrm{k}}(\mathscr{S}_1, \mathscr{S}_2) = L_{\mathrm{k}}(\mathscr{S}_2, \mathscr{S}_1)$.
(iii) If two curves are unlinked, then their linking number is zero.
(iv) If we change the orientation of one of the curves then $L_{\mathrm{k}}(\mathscr{S}_1, \mathscr{S}_2)$ will change sign. Changing the orientation of $\mathscr{S}_1$ can be achieved by reversing the direction of $\mathbf{e}_{t_1}$.
(v) The linking number of two curves is invariant to continuous deformations of the curves as long as the two curves are not allowed to pass through each other. That is, the linking number is a topological invariant.

We remark that many of these properties are illustrated by the examples shown in Figures 3.1 and 3.9. For instance, we can continuously deform the ellipses to other ellipses in Figure 3.9(a) and not change the linking number (i.e., (v) above). Although the ellipse $\mathscr{S}_2$ shown in Figure 3.9(a) can be continuously transformed into the ellipse $\mathscr{S}_2$ shown in Figure 3.9(c), the orientation of the transformed ellipse will differ from that of $\mathscr{S}_2$ shown in Figure 3.9(c) and, as a result (from (iv) above), the linking number will differ by a sign. The difference in sign is in agreement with the numerical computations that used Eqn. (3.28). Cutting one of the ellipses and then gluing it back together so that the curves in Figure 3.9(a) transform to those in Figure 3.9(b) would result in a change in the linking number but such a possibility does not contradict (v). Property (iv) is the reason why the linking numbers in the caption for Figure 3.1 are given as $\pm$: for these pairs of curves the directions of $\mathbf{e}_{t_1}$ and $\mathbf{e}_{t_2}$ were not prescribed and so two values of the linking number are possible depending on the choices of $\mathbf{e}_{t_1}$ and $\mathbf{e}_{t_2}$.

3.4 Total Geometric Torsion of a Space Curve and Total Twist of a Ribbon

Interest in the linking number of two space curves took on a new lease of life in the 1960s when a theorem by Călugăreanu showed that this quantity could be decomposed into the sum of two quantities known as twist and writhe. In preparation for discussing his wonderful theorem, we first pause to discuss measures of twist in space curves and rods.

To proceed, we recall that any space curve $\mathscr{S}$ (which is not necessarily closed) can be endowed with a Frenet triad and that this triad has an associated Darboux vector. We define the total geometric torsion of a space curve of length ℓ as the integral of the geometric torsion:

$$T_{\mathrm{w}}(\mathscr{S},\mathbf{e}_n)=\frac{1}{2\pi}\int_0^{\ell}\boldsymbol{\omega}_{\mathrm{SF}}\cdot\mathbf{e}_t\,ds. \tag{3.35}$$

Here, s is the arc-length parameter of $\mathscr{S}$ and this parameter varies from 0 to ℓ on $\mathscr{S}$. The division by 2π is a convention. With the help of the Serret-Frenet relations we note that the geometric torsion $\tau=\boldsymbol{\omega}_{\mathrm{SF}}\cdot\mathbf{e}_t$ and can be considered as the rate at which the normal vector $\mathbf{e}_n$ rotates about the tangent vector $\mathbf{e}_t$.

Now suppose ℓ and $\mathscr{S}$ are such that the tangent indicatrix c_t of the curve $\mathscr{S}$ forms a closed curve on the unit sphere. From our earlier discussion on the Gauss-Bonnet theorem we are aware that (cf. Eqn. (3.24))

$$\oint_{c_t}\kappa_g\,d\bar{s}+A=2\pi\qquad\text{modulo } 4\pi. \tag{3.36}$$

However, we also showed previously (cf. Eqn. (3.23)) that $\kappa_g\,d\bar{s}=\tau ds$. Thus,

$$\int_0^{\ell}\tau ds+A=2\pi\qquad\text{modulo } 4\pi. \tag{3.37}$$

Whence, the total geometric torsion can be related to the spherical area enclosed by the tangent indicatrix:

$$T_{\mathrm{w}}(\mathscr{S},\mathbf{e}_n)+\frac{A}{2\pi}=1\qquad\text{modulo } 2. \tag{3.38}$$

This relation was first recorded by Fuller [111, Eqn. (6.3)].[6]

Let us consider as an example a helical space curve[7]:

$$\kappa=\frac{1}{R(1+\alpha^2)}=\frac{1}{R}\cos^2(\varsigma),\qquad \tau=\frac{\alpha}{R(1+\alpha^2)}=\frac{1}{R}\cos(\varsigma)\sin(\varsigma), \tag{3.39}$$

[6] Fuller's version of Eqn. (3.38) differs from ours in that $T_{\mathrm{w}}(\mathscr{S},\mathbf{e}_n)$ is replaced by the more general case $T_{\mathrm{w}}(\mathscr{S},\mathbf{u})$ in Eqn. (3.38). Alternative proofs of Fuller [111, Eqn. (6.3)] can be found in Aldinger et al. [7] and Kamien [176].

[7] The parameters for this curve are discussed in Section 1.3.4.

where $\varsigma = \arctan(\alpha)$ is the pitch angle of the helix. If we parameterize the helix with the angle ϕ, then

$$\frac{d\phi}{ds} = \frac{1}{R\sqrt{1+\alpha^2}} = \frac{\cos(\varsigma)}{R}. \tag{3.40}$$

Consequently, for one segment of the helix,

$$\begin{aligned} T_{\mathrm{w}}(\mathscr{S}, \mathbf{e}_n) &= \frac{1}{2\pi}\int_0^{\ell} \boldsymbol{\omega}_{\mathrm{SF}} \cdot \mathbf{e}_t ds \\ &= \frac{1}{2\pi}\int_0^{\ell} \tau ds \\ &= \frac{1}{2\pi}\int_0^{2\pi} \tau R\sqrt{1+\alpha^2} d\phi \\ &= \frac{\alpha}{\sqrt{1+\alpha^2}} \\ &= \sin(\varsigma). \end{aligned} \tag{3.41}$$

The total geometric torsion $T_{\mathrm{w}}(\mathscr{S}, \mathbf{e}_n)$ is used to characterize configurations of double-stranded DNA. For the aforementioned segment of the helix, the tangent indicatrix forms a closed curve on the sphere. Thus, with the help of Fuller's identity (3.38), we find that the solid angle A enclosed by c_t is

$$A = 2\pi(1 - \sin(\varsigma)), \tag{3.42}$$

a result that, as expected, is in agreement with our earlier calculation of this solid angle in Section 3.2.2.

The aforementioned integral of the rate at which $\mathbf{e}_n$ rotates about $\mathbf{e}_t$ can also be applied to the frame $\{\mathbf{e}_t, \mathbf{u}, \mathbf{e}_t \times \mathbf{u}\}$ that we previously used to generate a ribbon (cf. Page 98 and Figure 3.6). Following classic works in this area such as [110, 213], the resulting integral is known as the total twist and it depends on both $\mathscr{S}$ and the choice of $\mathbf{u}$:

$$T_{\mathrm{w}}(\mathscr{S}, \mathbf{u}) = \frac{1}{2\pi}\int_0^{\ell} \boldsymbol{\omega}_t \cdot \mathbf{e}_t ds. \tag{3.43}$$

When $\mathbf{u} = \mathbf{e}_n$, then the total twist corresponds to the total torsion $T_{\mathrm{w}}(\mathscr{S}, \mathbf{e}_n)$ defined earlier. By way of comparison, if $\mathbf{u} = b_1\mathbf{B}_1 + b_2\mathbf{B}_2$ where $b_{1,2}$ are constants and $\mathbf{B}_{1,2}$ are the normal vectors associated with the Bishop frame, then

$$T_{\mathrm{w}}(\mathscr{S}, b_1\mathbf{B}_1 + b_2\mathbf{B}_2) = \frac{1}{2\pi}\int_0^{\ell} \boldsymbol{\omega}_{\mathrm{B}} \cdot \mathbf{e}_t ds = 0. \tag{3.44}$$

This result is the motivation for referring to the Bishop frame as a rotation minimizing frame. In the sequel, when specifying the twist, to avoid ambiguity where it might occur, we will specify the vector we are using to compute T_{w}.

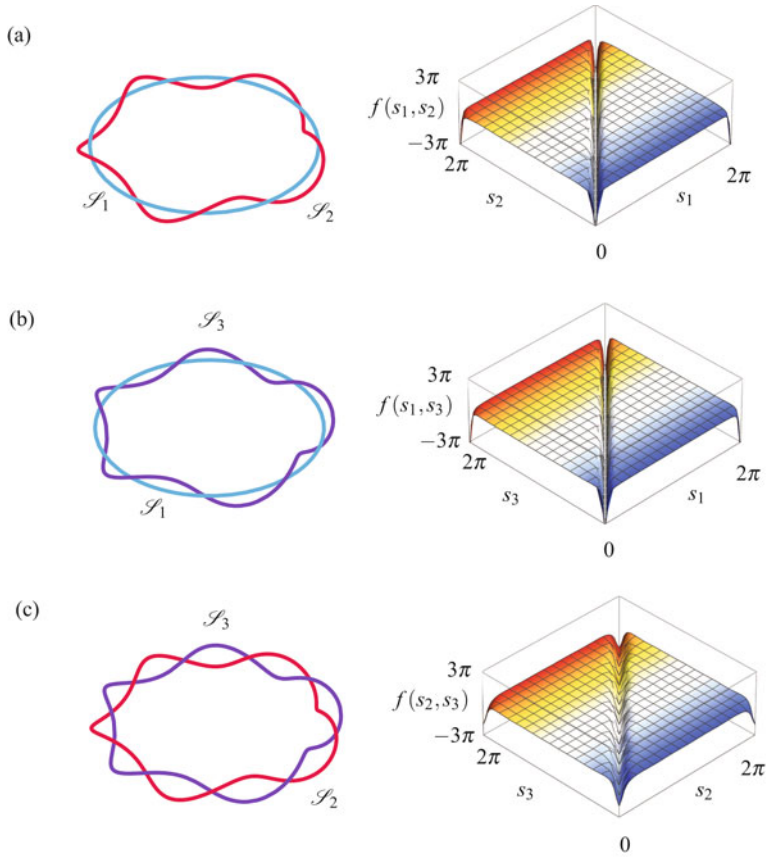

Fig. 3.11 Three distinct examples of a pair of space curves $\mathscr{S}$ and $\mathscr{S}_\varepsilon$ showing the behavior of the associated linking function $f(s_1,s_2)$ (cf. Eqn. (3.29)). For (a), $L_k(\mathscr{S}=\mathscr{S}_1,\mathscr{S}_\varepsilon=\mathscr{S}_2)=-5$; for (b), $L_k(\mathscr{S}=\mathscr{S}_1,\mathscr{S}_\varepsilon=\mathscr{S}_3)=-5$; and, for (c), $L_k(\mathscr{S}=\mathscr{S}_1,\mathscr{S}_\varepsilon=\mathscr{S}_3)=-5$. The linking number $L_k(\mathscr{S}_1,\mathscr{S}_\varepsilon)$ is defined by Eqn. (3.28). The curve $\mathscr{S}_1$ is a circle of radius 1 lying in the $x-y$ plane. The curves $\mathscr{S}_2$ and $\mathscr{S}_3$ are constructed as ribbons using the unit normal vector to $\mathscr{S}_1$ (cf. Eqn. (3.52) with $n=5$ and $\varepsilon=0.1$).

3.5 Călugăreanu's Theorem

Consider a closed ribbon formed from a pair of curves $\mathscr{S}$ and $\mathscr{S}_\varepsilon$. As indicated by the three examples shown in Figure 3.11, the curve $\mathscr{S}_\varepsilon$ is formed in the usual manner from the closed curve $\mathscr{S}$ using a unit vector $\mathbf{u}$ that is normal to $\mathbf{e}_t$ and a number ε.[8] Following standard practice, ε is considered to be sufficiently small so that the curves $\mathscr{S}$ and $\mathscr{S}_\varepsilon$ do not intersect. For such a ribbon, Călugăreanu [42–44]

[8] The orientability condition on the ribbon is satisfied when $\mathbf{u}(s)=\mathbf{u}(s+\ell)$ where $s\in[0,\ell]$ on $\mathscr{S}$. Thus, the ribbon is not a Möbius strip.

showed that the linking number could be decomposed additively into the sum of a quantity known as the writhe and the total geometric torsion:

$$L_k(\mathscr{S},\mathscr{S}_\varepsilon) = W_{\mathrm{r}}(\mathscr{S}) + T_{\mathrm{w}}(\mathscr{S},\mathbf{e}_n) + N(\mathscr{S},\mathscr{S}_\varepsilon). \tag{3.45}$$

In this equation,[9]

$$W_{\mathrm{r}} = W_{\mathrm{r}}(\mathscr{S}) = \frac{1}{4\pi}\oint_0^\ell \oint_0^\ell [\mathbf{e}_t(s_1)\times\mathbf{e}_t(s_2)]\cdot\frac{\mathbf{r}(s_1)-\mathbf{r}(s_2)}{\|\mathbf{r}(s_1)-\mathbf{r}(s_2)\|^3}ds_1 ds_2, \tag{3.46}$$

and $N(\mathscr{S},\mathscr{S}_\varepsilon)$ denotes the number of times $\mathbf{u}$ revolves about $\mathbf{e}_t$. Thus, if we define an angle ψ,

$$\mathbf{u} = \cos(\psi)\mathbf{e}_n + \sin(\psi)\mathbf{e}_b, \tag{3.47}$$

then, from [43],

$$N(\mathscr{S},\mathscr{S}_\varepsilon) = \frac{1}{2\pi}(\psi(\ell)-\psi(0)). \tag{3.48}$$

As noted by Moffatt and Ricca [239], the presence of $N(\mathscr{S},\mathscr{S}_\varepsilon)$ in Eqn. (3.45) accommodates the fact that the ribbon is formed with $\mathbf{u}$ which is not necessarily equal to $\mathbf{e}_n$. We refer to Eqn. (3.45) as Călugăreanu's theorem.

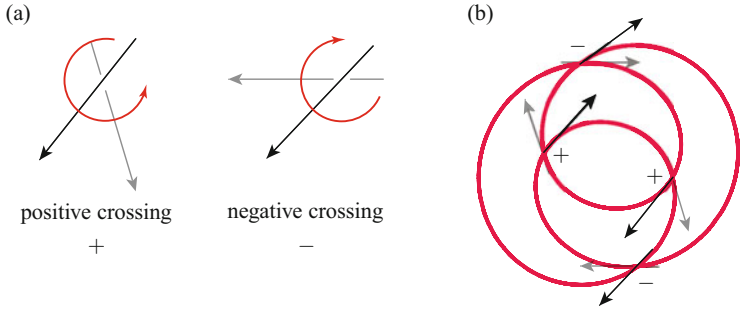

Fig. 3.12 (a) Conventions for the index $\mathscr{J}_W(\mathscr{P})$ of the signed crossings of a curve with itself. These representations are a more compact version of the index conventions for $J(\mathscr{P})$ shown earlier in Figure 3.10. (b) Example of the use of the convention with a particular projection of a figure eight knot.

The writhing number $W_{\mathrm{r}}(\mathscr{S})$ can be loosely interpreted as the number of times the curve $\mathscr{S}$ folds or coils upon itself. Complementing this nonlocal behavior, $T_{\mathrm{w}}(\mathscr{S},\mathbf{e}_n) + N(\mathscr{S},\mathscr{S}_\varepsilon)$ is a measure of the twisting of the ribbon about $\mathscr{S}$. The beauty of Călugăreanu's theorem is that it states that the sum of these two quantities is equal to the (invariant) linking number of the two curves. Thus, any deformations of the ribbon performed that change $W_{\mathrm{r}}(\mathscr{S})$ will induce an equal and opposite effect

[9] As emphasized in [7], the domain of integration excludes those points $s_1 = s_2$ where the integrand becomes unbounded.

in $T_{\mathrm{w}}(\mathscr{S},\mathbf{e}_n)+N(\mathscr{S},\mathscr{S}_\varepsilon)$. Thus, Eqn. (3.45) enables an intuitive understanding of the conversion of twist to writhe and vice versa that is often found in deformation of long slender bodies such as telephone cords and lengths of surgical tubing. Of course this perspective is gained after two material curves in the slender body are identified with $\mathscr{S}$ and $\mathscr{S}_\varepsilon$. Such an identification is readily made in the case of double-stranded DNA where $\mathscr{S}$ and $\mathscr{S}_\varepsilon$ can be individually identified with one of the pair of sugar-phosphate backbone curves. Indeed, as evidenced by the works of Crick [77] and Pohl [293], it did not take long after Călugăreanu's work was published in the early 1960s for people to realize that his theorem could be applied to understand the coiling behavior of double-stranded DNA.

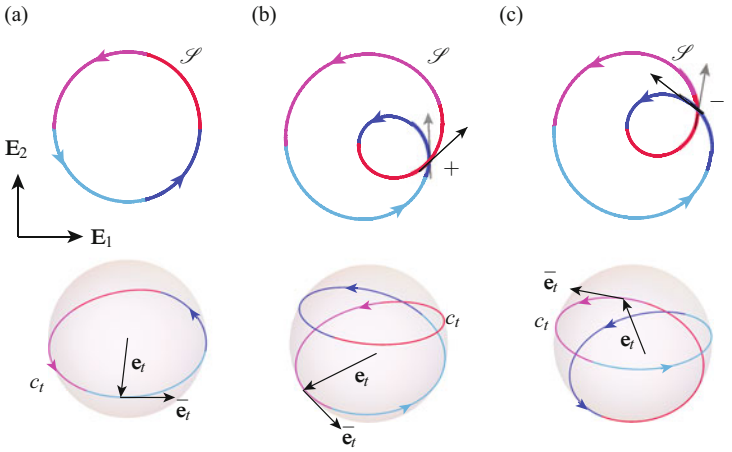

Fig. 3.13 Examples of calculations of $\mathscr{J}_W(\mathscr{P})$. (a), Closed curve with no crossings: $\mathscr{J}_W(\mathscr{P})=0$; (b), closed curve with a positive crossing: $\mathscr{J}_W(\mathscr{P})=1$; and (c), closed curve with a negative crossing: $\mathscr{J}_W(\mathscr{P})=-1$. The tangent indicatrices c_t for each of the three curves are also shown. Observe from (b) and (c) that when over- and under-crossings are interchanged the index changes by a factor of 2. The parametric expressions for $\mathscr{S}$ are taken from an example in [43] which is discussed further in Exercise 3.8.

In a highly cited paper that appeared in 1971, Fuller [110] introduced the term writhing number for $W_{\mathrm{r}}(\mathscr{S})$ because the verb to writhe is defined as "to twist into coils or folds." While the expression for the writhe integral has intriguing similarities to the definition (3.28) of the linking number of a pair of curves that was introduced earlier, it pertains only to the curve $\mathscr{S}$ and can take non-integer values. Computing $W_{\mathrm{r}}(\mathscr{S})$ has been the subject of many works since then. Several approaches can be found to this computation and each of them can offer a different perspective on $W_{\mathrm{r}}(\mathscr{S})$[10]:

[10] The primary reference for our summary of the methods used to compute the writhing number is [7]. We also recommend the later works [20, 21, 85, 169, 176] for helpful perspectives and insights on this topic.

(i) Taking advantage of a parametric representation for $\mathscr{S}$, if it is available, the integrand in Eqn. (3.46) can be evaluated directly. In this context, we note that parametric expressions for trefoil, figure eight, and other knots are readily available. We also note that if $\mathscr{S}$ is planar, then the triple product in the integrand in Eqn. (3.46) will be zero. Hence,

$$\text{For a planar curve } W_{\mathrm{r}} = 0. \tag{3.49}$$

(ii) Following Fuller [111], use Eqn. (3.45) to compute $W_{\mathrm{r}}(\mathscr{S})$ by first computing $L_k(\mathscr{S}, \mathscr{S}_\varepsilon)$ and $T_{\mathrm{w}}(\mathscr{S}, \mathbf{e}_n) + N(\mathscr{S}, \mathscr{S}_\varepsilon)$. The difference of these quantities then provides the sought after value of writhe:

$$W_{\mathrm{r}}(\mathscr{S}) = L_k(\mathscr{S}, \mathscr{S}_\varepsilon) - T_{\mathrm{w}}(\mathscr{S}, \mathbf{e}_n) - N(\mathscr{S}, \mathscr{S}_\varepsilon). \tag{3.50}$$

(iii) Again following Fuller [111], one uses the Gauss-Bonnet theorem to establish a relation between $T_{\mathrm{w}}(\mathscr{S}, \mathbf{e}_n)$ and the solid angle encircled by c_t (cf. Eqn. (3.38)). Then, after noting that $L_k(\mathscr{S}, \mathscr{S}_\varepsilon)$ is an integer, one appeals to Eqn. (3.45) to find

$$W_{\mathrm{r}}(\mathscr{S}) = L_k(\mathscr{S}, \mathscr{S}_\varepsilon) - 1 + \frac{A}{2\pi} - N(\mathscr{S}, \mathscr{S}_\varepsilon) \qquad \text{modulo 2.} \tag{3.51}$$

(iv) As summarized in [21], $W_{\mathrm{r}}(\mathscr{S})$ can be identified with the sum of the indices of the signed crossings of $\mathscr{S}$ with itself averaged over all possible projection angles. The convention for the index $\mathscr{J}_W(\mathscr{P})$ of the crossings is shown in Figure 3.12. The curve with no self-crossings has zero writhe, while the closed curves in Figure 3.13(b) & (c) show that by twisting a loop through 360°, a change in the writhing number can be achieved. The trefoil knots discussed in Exercise 3.9 offer an illustration of the invariance of writhing number to the choice of the direction of increasing arc-length parameter s.

3.6 Examples of Computing Writhing Numbers

To illuminate our comments on writhing numbers, it is necessary to explore some examples. One of the few works that we found where explicit computations could be found is in a paper by White and Bauer [360] and our examples are inspired by their work. Pairs of the space curves in question form ribbons, examples of which are shown in Figure 3.11. The three space curves which form the ribbons have parametric representations in terms of the arc-length parameter s_1 of $\mathscr{S}_1$[11]:

[11] The curves considered in [360] are discussed in Exercise 3.9.

$$\begin{aligned}
\mathbf{r}_1(s_1) &= \cos(s_1)\mathbf{E}_1 + \sin(s_1)\mathbf{E}_2,\\
\mathbf{r}_2(s_1) &= \mathbf{r}_1 + \varepsilon\left(\cos(ns_1)\cos(s_1)\mathbf{E}_1 + \cos(ns_1)\sin(s_1)\mathbf{E}_2 + \sin(ns_1)\mathbf{E}_3\right),\\
\mathbf{r}_3(s_1) &= \mathbf{r}_1 - \varepsilon\left(\cos(ns_1)\cos(s_1)\mathbf{E}_1 + \cos(ns_1)\sin(s_1)\mathbf{E}_2 + \sin(ns_1)\mathbf{E}_3\right),
\end{aligned} \tag{3.52}$$

where n and ε are constants. For the examples shown in Figure 3.11, $n = 5$ and $\varepsilon = 0.1$. Geometrically, the curves $\mathscr{S}_2$ and $\mathscr{S}_3$ wind counterclockwise about $\mathscr{S}_1$. As s_1 ranges from 0 to 2π, $\mathscr{S}_2$ winds n times around $\mathscr{S}_1$.

For the circle $\mathscr{S}_1$, we have

$$\mathbf{e}_{t_1} = -\sin(s_1)\mathbf{E}_1 + \cos(s_1)\mathbf{E}_2, \qquad \mathbf{e}_{n_1} = -\cos(s_1)\mathbf{E}_1 - \sin(s_1)\mathbf{E}_2, \qquad \mathbf{e}_{b_1} = \mathbf{E}_3, \tag{3.53}$$

and

$$\kappa_1 = 1, \qquad \tau_1 = 0. \tag{3.54}$$

For the helical spirals, some lengthy calculations reveal that

$$\begin{aligned}
\frac{ds_2}{ds_1} &= \sqrt{\varepsilon^2 n^2 + (1 + \varepsilon\cos(ns_1))^2} = 1 + \varepsilon\cos(ns_1) + O\left(\varepsilon^2\right),\\
\kappa_2 &= 1 + \varepsilon\left(n^2 - 1\right)\cos(ns_1) + O\left(\varepsilon^2\right),\\
\tau_2 &= 0 + \varepsilon n\left(1 - n^2\right)\cos(ns_1) + \varepsilon^2 n\left(n^2 - 1 + \left(n^4 + 3n^2 - 1\right)\cos(2ns_1)\right) + O\left(\varepsilon^3\right),\\
\mathbf{e}_{t_2} &= \mathbf{e}_{t_1} + \varepsilon n\left(\sin(ns_1)\,\mathbf{e}_{n_1} + \cos(ns_1)\,\mathbf{e}_{b_1}\right) + O\left(\varepsilon^2\right),\\
\mathbf{e}_{n_2} &= \mathbf{e}_{n_1} - \varepsilon n\left(\mathbf{e}_{t_1} + n\mathbf{e}_{b_1}\right)\sin(ns_1) + O\left(\varepsilon^2\right),\\
\mathbf{e}_{b_2} &= \mathbf{e}_{b_1} - \varepsilon n\left(\cos(ns_1)\,\mathbf{e}_{t_1} - n\sin(ns_1)\,\mathbf{e}_{n_1}\right) + O\left(\varepsilon^2\right).
\end{aligned} \tag{3.55}$$

The corresponding results for $\mathscr{S}_3$ can be obtained from Eqn. (3.55) by setting $\varepsilon \to -\varepsilon$. Thus for the three ribbons shown in Figure 3.11, we have the respective normal vectors that are used to define the ribbons:

$$\begin{aligned}
\mathbf{u}_1 &= -\cos(ns_1)\,\mathbf{e}_{n_1} + \sin(ns_1)\,\mathbf{e}_{b_1},\\
\mathbf{u}_2 &= -\mathbf{u}_1,\\
\mathbf{u}_3 &= 2\mathbf{u}_2 + O\left(\varepsilon^2\right).
\end{aligned} \tag{3.56}$$

The expressions (3.55) will now be used in conjunction with Eqn. (3.45) to obtain approximate expressions for the writhing numbers of the ribbons. For the third ribbon, extensive perturbation calculations are needed and we used a symbolic manipulation package for assistance.

To apply Călugăreanu's theorem (3.45), we compute using Eqns. (3.53) and (3.54) that

$$\begin{aligned}
T_{\mathrm{w}}(\mathscr{S}_1, \mathbf{e}_{n_1}) + N(\mathscr{S}_1, \mathscr{S}_2) &= N(\mathscr{S}_1, \mathscr{S}_2) = -n,\\
T_{\mathrm{w}}(\mathscr{S}_1, \mathbf{e}_{n_1}) + N(\mathscr{S}_1, \mathscr{S}_3) &= N(\mathscr{S}_1, \mathscr{S}_3) = -n.
\end{aligned} \tag{3.57}$$

By counting crossings and using Eqn. (3.34), we find that the linking numbers for these ribbons are also $-n$. Referring to Eqn. (3.50), this is consistent with the fact that the writhing number of the circle $\mathscr{S}_1$ is zero. Turning to the third ribbon, which is formed by $\mathscr{S}_2$ and $\mathscr{S}_3$, we find that $L_k(\mathscr{S}_2,\mathscr{S}_3) = -n$, $N(\mathscr{S}_2,\mathscr{S}_3) = -n$, and

$$\begin{aligned} T_{\mathrm{w}}(\mathscr{S}_2,\mathbf{e}_{n_2}) &= \frac{1}{2\pi}\int_0^{\ell_2}\tau_2 ds_2 \\ &= \frac{1}{2\pi}\int_0^{2\pi}\tau_2\frac{ds_2}{ds_1}ds_1 \\ &= \frac{\varepsilon}{2\pi}\int_0^{2\pi}\left(1-n^2\right)n\cos\left(ns_1\right)ds_1 \\ &+ \frac{\varepsilon^2 n}{4\pi}\int_0^{2\pi} n^2-1+\left(2n^4+5n^2-1\right)\cos\left(2ns_1\right)ds_1+O\left(\varepsilon^3\right) \\ &= \frac{\varepsilon^2 n}{2}\left(n^2-1\right)+O\left(\varepsilon^3\right). \end{aligned} \tag{3.58}$$

Consequently, using Călugăreanu's theorem (3.45), we compute the approximate expressions for the writhing numbers of the curves $\mathscr{S}_2$ and $\mathscr{S}_3$:

$$\begin{aligned} W_{\mathrm{r}}(\mathscr{S}_2) &= -\frac{\varepsilon^2 n}{2}\left(n^2-1\right)+O\left(\varepsilon^3\right), \\ W_{\mathrm{r}}(\mathscr{S}_3) &= -\frac{\varepsilon^2 n}{2}\left(n^2-1\right)+O\left(\varepsilon^3\right). \end{aligned} \tag{3.59}$$

For the curves shown in Figure 3.11, $W_{\mathrm{r}}(\mathscr{S}_2) \approx -1.2$.

The results of this analysis can be applied to circular strands of DNA (or DNA plasmids) that are discussed in the literature[12] provided the radius of the circular reference curve is used to non-dimensionalize the length scales. The radius R in this case is typically in the order of several hundred nanometers (nm) and εR is of the order of 1 nm.

3.7 Self-Linking of a Space Curve with Application to Strands of DNA

Restricting attention to curves with no points of inflection, Pohl [293] published the following identity for the self-linking number SL of the curve in 1968:

$$SL = W_{\mathrm{r}}(\mathscr{S}) + T_{\mathrm{w}}(\mathscr{S},\mathbf{e}_n), \tag{3.60}$$

[12] See [169, 360] and references therein.

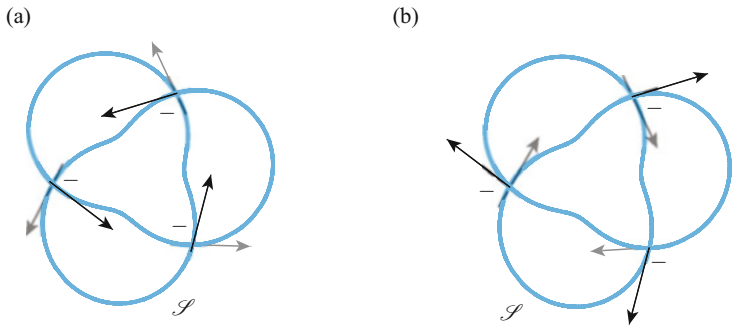

Fig. 3.14 A trefoil knot with a self-linking number $SL = -3$ showing the crossings for a given projection. (a) Computation of the crossing index using a given orientation of s and (b) computation by reversing the direction of s.

where SL is obtained from half the sum of the crossing indices $\mathscr{J}_W(\mathscr{P})$ of $\mathscr{S}$. As examples, $SL = -3$ for the trefoil knot shown in Figure 3.14, $SL = 0$ for the figure eight knot shown in Figure 3.12, and $SL = +1$ for the knot shown in Figure 3.13(c).

Pohl's student, White, subsequently extended Eqn. (3.60) in a well-cited paper [359]. In establishing Eqn. (3.60), Pohl was seeking to give "a new, clearer, and much simplified treatment of" Călugăreanu's theorem as presented in [42–44]. It should be clear that Eqn. (3.60) is intimately related to Călugăreanu's theorem (3.45). The identity (3.60) has also had an influential role in the literature on writhe and twist in rods and DNA.[13] There are numerous papers (e.g., [68, 235, 294, 314, 335]) devoted to this topic and, in particular, calculating W_{r} and T_{w} for deformed strands of DNA.

As mentioned previously, one of the primary drivers for the spread of interest in Călugăreanu's theorem (3.45) and Eqn. (3.60) has been an attempt to understand the supercoiling of DNA. To see how link, writhe, and twist can be applied to strands of double-stranded DNA (dsDNA), we recall that DNA can be modeled as two space curves $\mathscr{S}_1$ and $\mathscr{S}_2$ which are intertwined about a imaginary third curve $\mathscr{S}$ which is known as the duplex or molecular axis. We can define a ribbon using $\mathscr{S}$ and $\mathscr{S}_1$ (or $\mathscr{S}_2$). It is also interesting to note that dsDNA can also be found in closed configurations (called DNA circles or DNA plasmids). For example, the chromosome of the bacteria *E. Coli* is a DNA circle one millimeter in length, and has a linking number that is close to 300,000 [294].

The twisting number T_{w} of the DNA strand is calculated using the ribbon formed by $\mathscr{S}$ and $\mathscr{S}_{1,2}$, and the linking number L_{k} is also determined using the two space curves. It is standard to then apply Călugăreanu's theorem (3.45) to determine the writhe of the DNA strand.[14]

[13] We refer the reader to [239] for a discussion of Călugăreanu's legacy and the roles played by Călugăreanu's theorem and Eqn. (3.60).

[14] For examples, see [18, 360, 361].

For strands of DNA, one also defines the supercoiling density σ [83, 314]:

$$\sigma = \frac{L_{\mathrm{k}} - L_{\mathrm{k}_0}}{L_{\mathrm{k}_0}}. \tag{3.61}$$

Here, L_{k_0} is the self-linking number of a strand of DNA where the molecular axis (duplex axis) is straight and unstressed. For B-DNA, there are 10.5 base pairs per turn of the helix, so when the molecular axis is straight and unstressed, $W_{\mathrm{r}} = 0$ and

$$L_{\mathrm{k}_0} = T_{\mathrm{w}} = \frac{\text{Number of base pairs}}{10.5}. \tag{3.62}$$

For DNA in vivo, $\sigma = 0.5$ and $\sigma = -1.0$ for separated strands of double-stranded DNA. Strands of DNA, where $\sigma < 0 (> 0)$ are known as underwound (supercoiled).[15]

We emphasize that the twist T_{w} is the number of times that one sugar phosphate backbone wraps around the molecular axis $\mathscr{S}$ and the writhe W_{r} is the average of the indices of the self-crossings of the double helix. In many of the recent experiments on DNA, one fixes L_{k} (i.e., σ) and varies T_{w} by extending the strands of DNA (see, e.g., [40, 314, 335]). In this way, L_{k} is a control parameter for their experiments. A lucid discussion on the importance of using L_{k} in this manner can be found in Pohl [294].

Because the linking number is a topological invariant, the only way to change it is to cut the DNA strands. This is precisely what some enzymes known as *topoisomers* perform [83, 241]. Indeed, there are two types of these enzymes, which either cut one strand (Type I) or two strands (Type II). The former enable changes in L_{k} of $+1$ while the latter enable changes of $+2$. An example of the latter phenomenon can be seen in Figure 3.13 where the self-linking number SL for two curves differs by a factor of 2.

3.8 Exercises

Exercise 3.1: Consider a plane curve $y = f(x)$. For this curve, compute the tangent indicatrix c_t and its geodesic curvature κ_g. Verify that c_t describes a geodesic (i.e., a curve of shortest distance between two points) on the sphere S^2.

Exercise 3.2: Consider a left-handed circular helix ($\alpha < 0$) parameterized using a cylindrical polar coordinate system: $z = \alpha R\theta$. Compute the tangent indicatrix c_t for this helix and show that the Gauss-Bonnet theorem (3.24) can be used to compute the spherical area enclosed by c_t.

Exercise 3.3: While the linking number of two non-linked curves is zero (see, e.g., Figure 3.9(b)), the converse is not true. To see this fact, show that the linking number

[15] Underwound is also termed negatively supercoiled in contrast to the case $\sigma > 0$ which is termed positively supercoiled.

for the pair of closed space curves forming a link variously known as "Maxwell's link" or the "Whitehead link" has a linking number of 0.[16]

Exercise 3.4: Verify the computation of the linking number for the three pairs of curves shown in Figure 3.9 using the signed crossing formula (3.34). In your solution you might notice the difference in orientation between the curve labeled $\mathscr{S}_2$ that is shown in Figures 3.9(a) and 3.9(c).

Exercise 3.5: After suitably modifying the definition (3.28), compute the linking number of the following pair of curves which are defined parametrically by the respective position vectors:

$$\mathbf{r}_1 = \mathbf{r}_1(s_1) = s_1\mathbf{E}_1 + \mathbf{E}_3, \qquad \mathbf{r}_2 = \mathbf{r}_2(s_2) = s_2\mathbf{E}_2. \tag{3.63}$$

Exercise 3.6: After suitably modifying the definition (3.28), show that the linking number of two parallel lines is zero.

Exercise 3.7: Verify the identity (3.32). The following tensor, which describes a combined projection and scaling, will be useful in your work:

$$\mathbf{A} = \frac{1}{\|\mathbf{r}_1(s_1) - \mathbf{r}_2(s_2)\|}(\mathbf{I} - \mathbf{e}\otimes\mathbf{e}). \tag{3.64}$$

Here, from Eqn. (3.27),

$$\mathbf{e}(s_1, s_2) = \frac{\mathbf{r}_1(s_1) - \mathbf{r}_2(s_2)}{\|\mathbf{r}_1(s_1) - \mathbf{r}_2(s_2)\|}. \tag{3.65}$$

You will also find that the adjugate, $\mathrm{adj}(\mathbf{A})$, of the non-invertible tensor $\mathbf{A}$ is

$$\mathrm{adj}(\mathbf{A}) = \frac{1}{\|\mathbf{r}_1(s_1) - \mathbf{r}_2(s_2)\|^2}\mathbf{e}\otimes\mathbf{e}, \tag{3.66}$$

and plays a role in the derivation because of the identity

$$\mathrm{adj}(\mathbf{A})(\mathbf{a}\times\mathbf{b}) = \mathbf{A}\mathbf{a}\times\mathbf{A}\mathbf{b}, \tag{3.67}$$

which holds for any pair of vectors $\mathbf{a}$ and $\mathbf{b}$.

Exercise 3.8: Consider the following parametric equation for a closed space curve that appeared in Călugăreanu [43, Pages 616–617]:

$$x(t) = \cos(t) - \lambda\cos(2t), \quad y(t) = \sin(t) - \lambda\sin(2t), \quad z(t) = \alpha\lambda\sin(t). \tag{3.68}$$

In these expressions, the parameters $\lambda \geq 0$ and $\alpha = \pm 1$. Three examples of these curves are shown in Figure 3.13. Determine the unit tangent vector $\mathbf{e}_t$, arc-length parameter $s = s(t)$, curvature κ, and torsion τ for this space curve. In addition, show

[16] This result was first established by Maxwell [95, 301].

that there are no self-crossings provided $0 \leq \lambda < 0.5$, while for $\lambda > 0.5$ show that there is a self-crossing which can change sign depending on the whether $\alpha = \pm 1$.

Exercise 3.9: Consider the following pair of curves that are discussed in White and Bauer [360, Eqn. (16)]:

$$\begin{aligned}\mathbf{r}_1(s_1) &= R_A \cos(s_1)\mathbf{E}_1 + R_A \sin(s_1)\mathbf{E}_2,\\ \mathbf{r}_2(s_1) &= \mathbf{r}_1 - r\left(\cos(ns_1)\cos(s_1)\mathbf{E}_1 + \cos(ns_1)\sin(s_1)\mathbf{E}_2 - \sin(ns_1)\mathbf{E}_3\right).\end{aligned} \tag{3.69}$$

Here, r and R_A are constants and n is an integer.[17] As s_1 ranges from 0 to 2π, show that $\mathscr{S}_2$ winds n times around $\mathscr{S}_1$. Using the results in Section 3.6 where appropriate, show that $L_k(\mathscr{S}_1, \mathscr{S}_2) = n$.

Exercise 3.10: As an alternative to the Frenet triad, Bishop [28] proposed a framing of the curve that is now known as the Bishop frame: $\{\mathbf{e}_t, \mathbf{B}_1, \mathbf{B}_2\}$. As discussed in Section 3.2, for this right-handed orthonormal frame $\mathbf{B}_1$ and $\mathbf{B}_2 = \mathbf{e}_t \times \mathbf{B}_1$ are chosen such that they only change in the direction of $\mathbf{e}_t$:

$$\frac{\partial \mathbf{B}_1}{\partial s} = -\kappa_{\mathrm{B}_1}\mathbf{e}_t, \qquad \frac{\partial \mathbf{B}_2}{\partial s} = -\kappa_{\mathrm{B}_2}\mathbf{e}_t. \tag{3.70}$$

Here, the curvatures κ_{B_1} and κ_{B_2} are functions of s. The present exercise explores the Bishop frame for the plane curve

$$\mathbf{r} = x\mathbf{E}_1 + f(x)\mathbf{E}_2, \tag{3.71}$$

where f is a sufficiently smooth function of x. The results of the exercise will reveal the advantage of the Bishop frame when a curve has an inflection point, and the nonuniqueness of the vectors $\mathbf{B}_1$ and $\mathbf{B}_2$.

(a) Consider the plane curve $\mathbf{r} = x\mathbf{E}_1 + f(x)\mathbf{E}_2$ shown in Figure 3.3. For this curve, show that the unit tangent vector has the representation

$$\mathbf{e}_t = \frac{1}{\sqrt{1 + \frac{df}{dx}\frac{df}{dx}}}\left(\mathbf{E}_1 + \frac{df}{dx}\mathbf{E}_2\right), \tag{3.72}$$

and the curvature κ is

$$\kappa = \frac{\left|\frac{d^2 f}{dx^2}\right|}{\left(\sqrt{1 + \frac{df}{dx}\frac{df}{dx}}\right)^3}. \tag{3.73}$$

(b) For the plane curve, show that two possible choices of the Bishop frame are

$$\{\mathbf{e}_t, \mathbf{B}_1 = \mathbf{n}_1, \mathbf{B}_2 = \mathbf{E}_3\}, \qquad \{\mathbf{e}_t, \mathbf{B}_1 = -\mathbf{n}_1, \mathbf{B}_2 = -\mathbf{E}_3\}, \tag{3.74}$$

[17] The curve $\mathscr{S}_2$ is not identical to the curve $\mathscr{S}_2$ that is defined in Eqn. $(3.52)_2$.

where the unit vector

$$\mathbf{n}_1 = \frac{1}{\sqrt{1+\frac{df}{dx}\frac{df}{dx}}}\left(\mathbf{E}_2 - \frac{df}{dx}\mathbf{E}_1\right). \tag{3.75}$$

For this pair of frames, show the respective results:

$$\kappa_{\mathrm{B}_1} = \frac{\frac{d^2f}{dx^2}}{\left(\sqrt{1+\frac{df}{dx}\frac{df}{dx}}\right)^3}, \qquad \kappa_{\mathrm{B}_2} = 0, \tag{3.76}$$

and

$$\kappa_{\mathrm{B}_1} = -\frac{\frac{d^2f}{dx^2}}{\left(\sqrt{1+\frac{df}{dx}\frac{df}{dx}}\right)^3}, \qquad \kappa_{\mathrm{B}_2} = 0. \tag{3.77}$$

In contrast to the Frenet triad, observe that each of these frames is defined even at points where the curvature $\kappa = 0$ (i.e., at a point of inflection). It is also interesting to note that, for both Bishop frames, the angle θ_{B} (defined by Eqn. (3.9)) is either 0° or 180° and switches between these values at points of inflection.

(c) Show that

$$\mathbf{B}_1 = \cos(\theta_0)\,\mathbf{n}_1 + \sin(\theta_0)\,\mathbf{E}_3, \qquad \mathbf{B}_2 = -\sin(\theta_0)\,\mathbf{n}_1 + \cos(\theta_0)\,\mathbf{E}_3, \tag{3.78}$$

where θ_0 is a constant, satisfy the conditions (3.70) with

$$\kappa_{\mathrm{B}_1} = \frac{\frac{d^2f}{dx^2}\cos(\theta_0)}{\left(\sqrt{1+\frac{df}{dx}\frac{df}{dx}}\right)^3}, \qquad \kappa_{\mathrm{B}_2} = \frac{\frac{d^2f}{dx^2}\sin(\theta_0)}{\left(\sqrt{1+\frac{df}{dx}\frac{df}{dx}}\right)^3}. \tag{3.79}$$

These results demonstrate statements in Bishop [28, Section 3] that the Bishop frame is not unique and that κ_{B_1} and κ_{B_2} are determined up to a rotation.

(d) Compute Bishop frames for a circular arc and compare the frames to the Frenet triad. Your results should be consistent with Eqn. (3.15).